REVIEW OF RESEARCH

ISSN: 2249-894X
IMPACT FACTOR : 5.7631(UIF)
UGC APPROVED JOURNAL NO. 48514
VOLUME - 8 | ISSUE - 8 | MAY - 2019

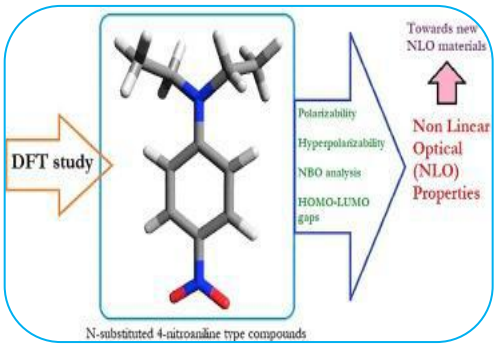

"VIBRATIONAL SPECTRAL STUDIES, DFT BASED QUANTUM CHEMICAL PARAMETERS AND NONLINEAR OPTICAL PROPERTIES OF 3-DIMETHYLAMINOANISOLE AS PI-SPACER WITH DONOR AND ACCEPTOR VARIATIONS EFFECT FOR DYE-SENSITIZED SOLAR CELLS ENACTMENT"

M. Anuradha[a], M. Karnan[a] , M. Karunanidhi[a] , V. Sivagami[a] and R. Meenakshi[b]

[a]PG& Research Department of Physics, Srimad Andavan Arts & Science College (Autonomous), Trichy, Tamil Nadu, India.
[b]PG Department of Physics, Cauvery College for Women, Trichy, Tamil Nadu, India.

ABSTRACT:

The present work attention on the design and enlargement of new 3-Dimethylaminoanisole (3DMA) derivatives in alternate Donor-Acceptor (D-A) structure for solar cells applications. Six molecules based on 3DMA combined with the electron-rich benzene and triphenylamine (TPA) units have been investigated using the DFT and TD-DFT methods with B3LYP functional implemented with 6-31+G(d, p) basis set. These results indicate that the extension of pi-conjugation can efficiently improve the absorption intensity. This simulation is estimated to assist the design, high - performance dyes for dye-sensitized solar cells (DSSC) applications. This work presents a systematic investigation of the nonlinear optical properties of 3DMA. The FT-IR and FT-Raman spectra of 3-Dimethylaminoanisole have been recorded. The vibrational frequencies of the title compound were obtained theoretically by DFT/B3LYP calculations employing the standard 6-31+G(d,p) and cc-pVTZ basis set for optimized geometry and was compared with observed spectrums.

KEYWORDS: *TD-DFT, Donor-Acceptor, Solar cell, LHE.*

INTRODUCTION:

Methoxy group, anisole is a hydrogen-bond acceptor molecule, whose aromatic ring is more electron-rich than that in benzene. In such kind of molecules, the role of the substituents is very important. Owing to the symmetry properties and also because of the limited information about the molecular parameters, reliable theoretical calculations for such a molecule is not possible. Therefore, it was thought worthwhile to understand the role of the substituents.Dye-sensitized solar cells (DSSCs) have concerned substantial attention as prospective low-cost replacements to silicon-based photovoltaic technology [1]. High-performance sensitizers capable of wide-band spectral capture are recognized to be a promising strategy for improving the cost-efficiency of the DSSCs. From this, organic sensitizers are recognized to be ideal for traditionally used sensitizers. The organic dyes have stronger light harvesting efficiency because of their high molar extinction coefficient. In general solar dye-design encompasses donor linked to an electron acceptor attaching functionality which permits fine-tuning of optical and electrochemical properties. For donors, benzene and triphenylamines [2, 3], have been successfully used. The electron acceptor anchoring functionality may be chosen as cyanoacrylic acid, nitro and carboxylic acid group functionality are being developed and optimized by several research groups.
Quantum chemical methods have

already proven to be very useful in determining the molecular structure and reactivity [4]. Density functional theory (DFT) [5, 6] has given a very suitable outline for emerging different standards for streamlining, forecasting, and ultimately understanding several features of chemical methods [7-11]. Different kinds of chemical perceptions that are presently used as descriptors of chemical reactivity ie., hardness or softness quantities, electronegativity [8] etc., appear obviously within DFT. The Fukui function [10] signifying the local softness of the electron in gas phase, measures the local electron density population displacements admire the flow of a single electron.

Due to these applications and the unswerving properties of anisole, a complete vibrational study of 3-Dimetylaminoanisole (3DMA) is undertaken. It has been reported the geometrical structure, quantum chemical calculations, charge distribution among atoms and surfaces, Global reactivity descriptors are also calculated to understand the reactive nature of the compound. Moreover, nonlinear optical, magnetic properties of 3DMA also studied using B3LYP/ 6-31+G (d, p) and cc-pVTZ basis set. On existent a temperately green solvent, anisole have been effectively pragmatic to process organic/polymer solar cells [12]. From this 3-Dimethylaminoanisole preferably bring in to produce good dye sensitizer.

2. EXPERIMENTAL DETAILS

The sample 3DMA was obtained from the Sigma Aldrich with a purity of greater than 97% and it was used as such without additional cleansing. The Fourier Transform Infrared (FT-IR) spectrum of the sample was recorded at room temperature in the region 4000-400 cm^{-1} using Perkin-Elmer spectrum1 spectrophotometer equipped with the composition of the pellet. The Fourier transform Raman (FT-Raman) BRUKER-RFS 27 spectrometer was used for the FT-Raman spectral measurements at room temperature. The sample was packed in a glass tube of about 5 mm diameter and excited in the 180° geometry with 1064 nm laser line at 100 MW power from a diode pumped air cooled-cwNd:YAG laser as an excitation wavelength in the region 4000-100 cm^{-1}.

3. COMPUTATIONAL DETAILS

Calculations of the title compound were carried out with Gaussian 09W program [13] using the DFT levels of theory using the standard B3LYP/ 6-31+G(d,p) & cc-pVTZ basis sets to predict the molecular structure and vibrational wavenumbers. Molecular geometry (Fig. 1) was fully optimized by optimization algorithm using redundant internal coordinates. The computed wavenumber values contain known systematic errors and hence, we have used the scaling factors 0.9613 and 0.9747 for 6-31+G (d, p) and cc-pVTZ basis sets, respectively [14]. The absence of imaginary wavenumbers of the calculated vibrational spectrum confirms that the structure deduced corresponds to minimum energy. The assignments of the calculated wavenumbers are aided by the animation option of GAUSSVIEW program, which gives a visual presentation of the vibrational modes [15]. The potential energy distribution (PED) is calculated with the help of MOLVIB program version 7.0 written by Sundius [16, 17].

4. RESULTS AND DISCUSSION

4.1. Molecular Geometry

Molecular structure of the 3DMA be applicable to C1 point group symmetry. The optimized molecular structure is took from GAUSSIAN 09W and GAUSSVIEW programs as shown in Fig.1, the compound encloses 2-methyl group and amino with anisole. The energy of the 3DMA at B3LYP/6-31+G (d, p) and cc-pVTZ levels are -480.724 and –480.913 Hartees respectively. Table 1 compares the calculated bond lengths and angles for 3DMA

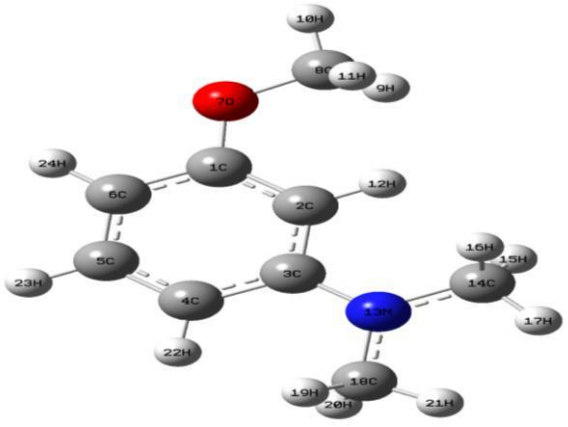

Fig.1 Optimized structure of 3-Dimethylaminoanisole

with those experimentally available from X-ray diffraction data [18].

Table 1. The selected bond lengths, bond angles for 3-dimethylaminoanisole

Parameters	Bond Length (Å)			Parameters	Bond Angle (deg)		
	6-31+ G(d,p)	cc-pVTZ	Expt. Value.*		6-31+ G(d,p)	cc-pVTZ	Expt. Value*
C1-C2	1.397	1.391	1.362	C2-C1-C6	121.045	120.889	120.7
C1-C6	1.402	1.396	1.384	C2-C1-O7	123.490	1 23.528	
C1-O7	1.371	1.366	1.370	C6-C1-O7	115.465	115.584	
C2-C3	1.419	1.412	1.427	C1-C2-C3	120.431	120.521	120.8
C2-H12	1.081	1.076		C1-C2-H12	119.756	119.704	
C3-C4	1.413	1.406	1.385	C3-C2-H12	119.813	119.775	
C3-N13	1.387	1.381		C2-C3-C4	118.257	118.203	119.9
C4-C5	1.397	1.389	1.363	C2-C3-N13	120.502	120.546	
C4-H22	1.083	1.078	1.080	C4-C3-N13	121.241	121.251	
C5-C6	1.391	1.383	1.440	C3-C4-C5	120.014	120.028	
C5-H23	1.088	1.083	1.080	C3-C4-H22	120.855	120.780	
C6-H24	1.085	1.080	1.080	C5-C4-H22	119.132	119.192	
O7-C8	1.419	1.415		C4-C5-C6	121.904	121.911	121.4
C8-H9	1.099	1.094	1.090	C4-C5-H23	118.798	118.819	
C8-H10	1.092	1.087	1.090	C6-C5-H23	119.298	119.270	
C8-H11	1.099	1.094	1.090	C1-C6-C5	118.349	118.448	118.5
N13-C14	1.451	1.447		C1-C6-H24	119.472	119.388	
N13-C18	1.452	1.448		C5-C6-H24	122.179	122.164	
C14-H15	1.101	1.096		C1-O7-C8	119.080	119.001	
C14-H16	1.101	1.096		O7-C8-H9	111.483	111.672	
C14-H17	1.092	1.087		O7-C8-H10	105.776	106.044	
C18-H19	1.100	1.095		O7-C8-H11	111.483	111.672	
C18-H20	1.100	1.095		H9-C8-H10	109.300	109.121	
C18-H21	1.092	1.087		H9-C8-H11	109.409	109.121	

4.2. Vibrational Assignments

The observed IR, Raman bands and calculated frequencies with assignments are given in Table 2. The observed and calculated FT-IR and FT-Raman spectra of 3DMA are shown in Fig. 2a & 2b respectively. The experimentally observed values are in agreement with that given by B3LYP/ 6-31+G (d, p) and cc-pVTZ basis set and hence the theoretical values of frequencies are discussed.

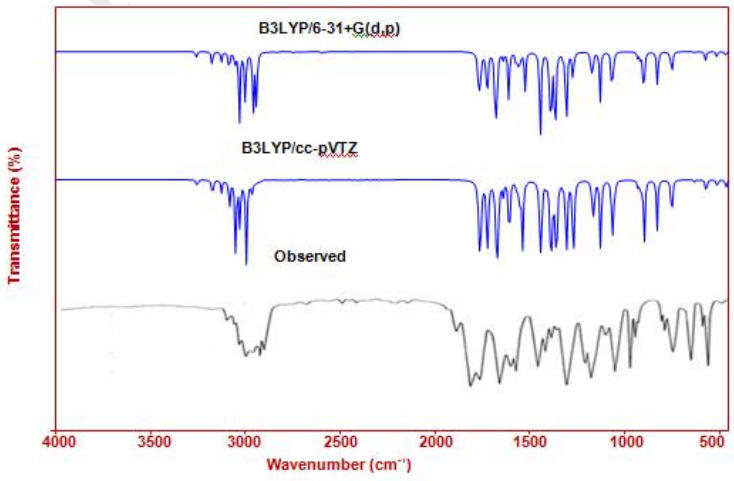

Fig. 2(a)Observed and simulated FT-IR spectra of 3-Dimethylaminonisole

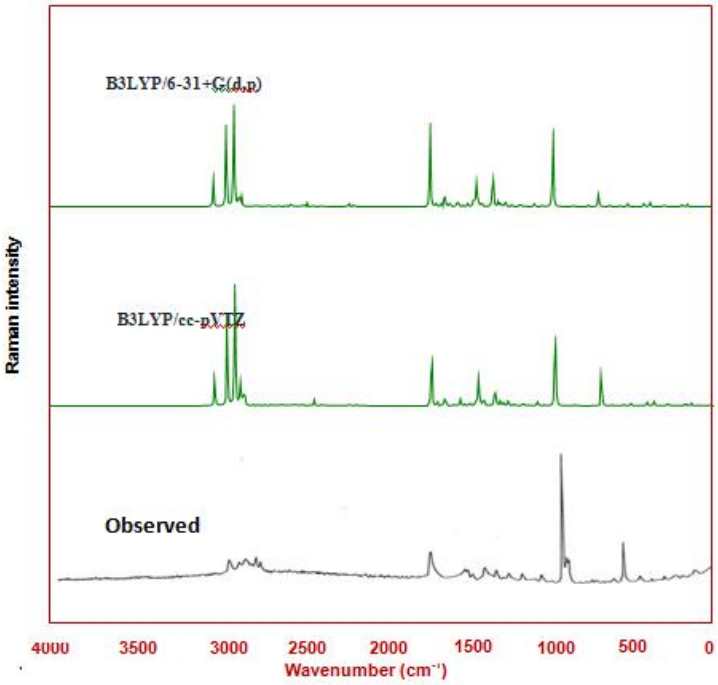

Fig.2(b)Observed and simulated FT-Raman spectra of 3-Dimethylaminoanisole

4.2.1. C-H vibrations

The hetero aromatic structure shows the presence of C-H stretching vibrations in the region 3100-3000 cm^{-1} which is the characteristic region for the C-H stretching vibrations [19]. Hence, the IR and Raman bands at 3000, 2955 & 3083, 3000, 2917 cm^{-1} in 3DMA have been assigned to C-H stretching vibrations. The scaled vibrations at 3089, 3084, 3008, 3006, 2962, 2960, 2922 cm^{-1} corresponds to stretching mode to CH unit. The C-H in plane bending vibration computed at 1322, 1219, 1185, 1093 cm^{-1} by cc-pVTZ method, even though found to be contaminated by CH_3 in plane bending are in the range found in literature [20, 21], while the experimental observations in FTIR at 1326 & 1093 cm^{-1} shows excellent agreement with theoretical value. The calculated frequencies at 863, 844, 827, 763 cm^{-1} for the CH out of plane bending falls in the FT-IR value at 860, 826, 756 cm^{-1} and FT-Raman value at 843, 757 cm^{-1}.

4.2.2. C-N vibrations

The identification of C-N vibrations is a very difficult assignment, since the mixing of several bands are possible in the region. Silverstein et al. [22] assigned C-N stretching absorption in the region 1382-1266 cm^{-1} for aromatic amaines. In this C-N stretching band are calculated to be present at 1352 and 1350 cm^{-1}, in FT-IR the band observed at 1349cm^{-1} respectively.

4.2.3. Methyl group vibrations

The compound under consideration 3- Dimethylaminoanisole possess a CH_3 group in the side substitution chain. There are nine fundamental one can except to a CH_3 stretching, the two asymmetrical CH_3 stretching, in-plane bending, out-of-plane bending, in-plane rocking, out-of-plane rocking, symmetric bending and torsion [23]. Methyl groups attached to unsaturated carbons including aromatic groups, absorb in the range 3010-2905 cm^{-1} due to the asymmetric stretching vibration, the symmetric stretching band occurring in the region 2945-2845 cm^{-1}. The FT- IR, FT-Raman band at 2886, 2841, 2795, 2477& 2861, 2833, 2788 cm^{-1} represents asymmetric and symmetric stretching vibrations of the methyl group in 3DMA.

Symmetric in-plane bending vibration have been identified at 1568, 1500, 1457 cm^{-1} in FT-IR and FT-Raman. Asymmetric in-plane bending vibration of CH_3 has been identified at 1442, 1443, 1414, 1357 cm^{-1}. The theoretically calculated value by B3LYP method using 6-31+G(d,p) and cc-pVTZ have been identified the asymmetric and symmetric in-plane bending modes of CH_3 group is tabulated.

Table 2. Experimental FT-IR, FT-Raman and Calculated DFT-B3LYP/6-31+G(d,p), cc-pVTZ levels of vibrational frequencies,of 3-Dimethylaminoanisole.

S.No	Observed frequencies (cm^{-1})		Calculated frequencies (cm^{-1})				Vibrational Assignments (%)
			B3LYP/6-31+ G(d,p)		B3LYP/cc-pVTZ		
	IR	Raman	Unscaled	Scaled	Unscaled	Scaled	
1		3083	3257	3089	3241	3084	νCH (100)
2	3000	3000	3233	3008	3220	3007	νCH (99)
3	2955		3219	2962	3202	2960	νCH (98)
4		2917	3183	2922	3167	2921	νCH (97)
5	2886		3150	2893	3129	2890	νCH_3ass(99)
6		2861	3151	2870	3122	2868	νCH_3ass(98)
7	2841		3136	2847	3115	2845	νCH_3ass(95)
8		2833	3078	2840	3051	2835	νCH_3ass(98)
9	2795		3041	2801	3018	2796	νCH_3ass(97)
10		2778	3034	2784	3011	2781	νCH_3ass(96)
11			3020	2634	2999	2630	νCH_3ss(99)
12	2477		3007	2481	2988	2479	νCH_3ss(98)
13	2227		2996	2235	2978	2234	νCH_3ss(97)
14	1648		1654	1659	1645	1657	νCC(76), δCH (17)
15	1614	1611	1629	1621	1621	1619	νCC(77)
16			1556	1578	1543	1571	νCC(78),σCH_3 (25)
17	1568		1549	1570	1534	1568	σCH_3 (65)
18			1540	1539	1523	1539	σCH_3 (58)
19	1500		1525	1511	1507	1508	σCH_3 (72)
20	1465		1515	1473	1503	1472	νCC(68)
21		1457	1514	1461	1494	1459	σCH_3 (85)
22			1511	1453	1487	1452	σCH_3 (73)
23	1442	1443	1503	1444	1482	1441	ρCH_3 (67)
24			1496	1429	1480	1425	σCH_3 (75)
25		1414	1482	1421	1470	1419	ρCH_3 (57), CC(27)
26		1357	1464	1357	1449	1356	ρCH_3 (77)
27	1349		1395	1352	1385	1350	νCN(78)
28	1326		1377	1322	1366	1322	δCH (87)
29		1300	1355	1307	1345	1303	νNCH_3(75),νCC(22)
30	1291		1290	1298	1276	1295	νNCH_3(78)
31		1271	1277	1277	1268	1272	νCO(72)
32	1233	1237	1215	1238	1209	1237	φCH_3 (82)
33			1204	1220	1196	1219	δCH (79)
34			1194	1187	1185	1185	δCH (51), φCH_3(43)
35		1171	1178	1177	1174	1175	φCH_3 (72)
36			1155	1160	1147	1152	φCH_3 (87)

37	1140		1143	1145	1138	1141	φCH_3 (83)
38	1093		1117	1097	1112	1093	δCH (75), φCH_3 (12)
39		1086	1089	1089	1082	1083	φCH_3 (88)
40	1047		1078	1050	1073	1048	νOCH_3(72), δCH (14)
41	988	986	1017	991	1018	989	δCC(68), νCO
42	977	971	993	980	993	978	δCC (81)
43	860		965	867	973	862	γCH (81)
44		857	883	861	882	859	δCN(68), νCC(17)
45		843	842	848	853	844	γCH(93)
46	826		822	829	835	827	γCH(83)
47	756	757	761	761	769	763	γCH(87)
48		700	716	699	717	694	δCC(81)
49	686		695	689	704	689	δCC(76)
50		629	631	628	637	630	γCC (71)
51		571	580	575	582	573	δOCH_3 (74), δCN (13)
52	558		557	562	556	557	δNCH_3 (80)
53		514	476	519	478	515	δNCH_3 (77)
54		457	465	461	468	459	γCC (65)
55		414	456	417	457	415	δCO(63)
56		371	384	379	381	372	γCC (55)
57			288	291	285	289	γCC (68)
58			287	286	282	284	γOCH_3(59)
59			271	280	265	281	γCN (68)
60			226	225	218	223	τCH_3 (85)
61			192	183	182	182	τCH_3 (75)
62			172	171	170	169	γCO (68)
63			146	146	139	140	τCH_3 (71)
64			89	93	93	90	$COCH_3$ torsion
65			54	58	55	59	γNCH_3(69)
66			23	24	25	24	γNCH_3(45)

ν-stretching, δ -in-plane bending, γ-out-of-plane bending, σ-scissoring, ρ-rocking, τ-twisting, φ-wagging

4.3. Molecular Electrostatic Potential (MESP) and Fukui function

The MESP and the Fukui function are reactivity indices of the identical feature, while they appear to be associated with different forms of features of the systems considered. Over MESP, Fukui function has greater sensitivity. The values of Fukui function are listed in Table 3. Parr and Yang [10] outlined the Fukui function, which might be written as the partial derivative of the electron density, with respect to the total number of electrons, taken at a constant external potential $f(r) = \left(\frac{\delta\mu}{\delta v(r)}\right)_N = \left(\frac{\delta\rho(r)}{\delta N}\right)_{v(r)}$

Table 3. Condensed Fukui functions for 3-Dimethylaminoanisole calculated at B3LYP/cc-pVTZ method.

Atom	q_k(N+1)	q_k(N)	q_k(N-1)	f_k^n	f_k^e	f_k^r	Δf_r
C1	-2.676	-0.389	-0.430	-2.287	0.041	-1.123	-2.329
C2	6.098	0.017	0.279	6.080	-0.262	2.909	6.342
C3	-6.431	0.526	0.380	-6.958	0.146	-3.406	-7.103
C4	1.939	0.061	0.130	1.878	-0.068	0.905	1.946
C5	-3.392	-0.655	-0.547	-2.737	-0.108	-1.423	-2.629
C6	2.172	-0.204	-0.058	2.376	-0.146	1.115	2.522
O7	-0.410	-0.388	-0.369	-0.023	-0.019	-0.021	-0.004
C8	-0.116	-0.316	-0.284	0.201	-0.033	0.084	0.233
H9	0.203	0.202	0.218	0.001	-0.016	-0.007	0.016
H10	0.196	0.205	0.246	-0.009	-0.041	-0.025	0.032
H11	0.203	0.202	0.218	0.001	-0.016	-0.007	0.016
H12	0.195	0.162	0.201	0.033	-0.038	-0.003	0.071
N13	-0.142	-0.219	-0.312	0.077	0.093	0.085	-0.015
C14	-0.037	-0.522	-0.454	0.485	-0.068	0.209	0.553
H15	0.199	0.212	0.254	-0.014	-0.042	-0.028	0.029
H16	0.199	0.212	0.254	-0.014	-0.042	-0.028	0.029
H17	0.203	0.196	0.231	0.007	-0.035	-0.014	0.042
C18	-0.460	-0.445	-0.390	-0.015	-0.055	-0.035	0.040
H19	0.187	0.214	0.255	-0.026	-0.042	-0.034	0.015
H20	0.187	0.214	0.255	-0.026	-0.042	-0.034	0.015
H21	0.208	0.192	0.229	0.016	-0.037	-0.010	0.053
H22	0.167	0.166	0.217	0.002	-0.051	-0.025	0.052
H23	0.149	0.173	0.232	-0.024	-0.059	-0.042	0.035
H24	0.159	0.182	0.244	-0.023	-0.062	-0.043	0.039

Due to the discontinuity of this derivative at the N value considered, it was proposed [10] to associate different reactivity indices to the equation above. These indices are, in a finite difference approximation

$$f^{-}(r) \approx \rho_N(r) - \rho_{N-1}(r)$$

in the case of an electrophilic attack on the system investigated, and $f^{+}(r) \approx \rho_{N+1}(r) - \rho_N(r)$ in the case of a nucleophilic attack. $\rho_N(r), \rho_{N+1}(r)$ and $\rho_{N-1}(r)$ are the electron density functions of the N, (N+1), (N-1) electron systems, all calculated at the geometry of the N-electron system. The function f^0, governing radical attack, is considered to be the average of f^+ and f^-.

A "condensed" version of the Fukui function was proposed by Yang and Mortier [24]. These atomic quantities f_k were defined in the gross atomic charges q_k at the atom k, obtained by Mulliken population analysis [25] for the N, (N+1), (N-1) electron system.

$f_k^+ = q_k(N+1) - q_k(N)$ and $f_k^- = q_k(N) - q_k(N-1)$

The positive values of f^- indicate high reactivity at the given

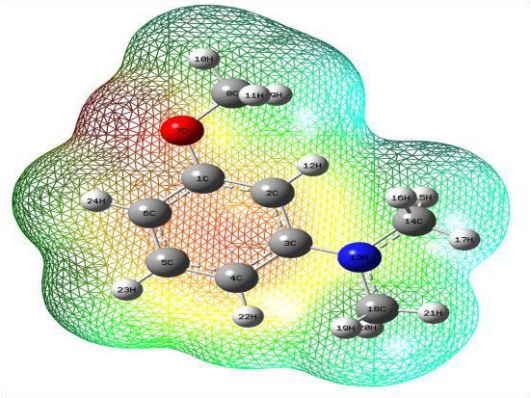

Fig. 3 MESP surface of 3-Dimethylaminoanisole

atom for the electrophilic attack within the plane perpendicular to the molecular plane of the substituted benzenes. The negative values of the f^- indicate that it is very unlikely for an electrophilic attack to take place in the molecular plane of the substituted benzenes. Within the framework of the HSAB theory formulated by Pearson [11], two important kinds of interaction between molecules can be distinguished. On one side the hard-hard interaction, which indicates that the reaction is primarily charge controlled, and on the other side the soft-soft interaction, which indicates that the reaction is primarily orbital controlled. Here MEP is a descriptor especially of the hard-hard interactions.

In the present work, 3D plots of molecular electrostatic potential (MESP) of 3DMA has been drawn in Fig. 3. The MESP is a plot of electrostatic potential mapped onto the constant electron density surface.The different values of the Electro Static Potential (ESP) at the surface are represented by different colours. In the title compound, where blue displays the strongest attraction and red gives the strongest repulsion.

4.4.. Magnetic moment and Magnetic susceptibility

Most organic and main group element compounds have all the electrons paired and these are diamagnetic molecules with very small magnetic moments. The number of unpaired electrons provides information about the oxidation state and electron configuration [26]. Magnetic moment is not measured directly. Calculation of moment can give useful chemical information. The values of magnetic moment for oxygen and nitrogen is listed in Table 4(a). Magnetic moment of the title compound is found to be 3.863 BM.

Table 4(a). Magnetic moment of 3-Dimethylaminoanisole accomplished at B3LYP/cc-PVTZ.

Ions	Number of lone pairs	Magnetic moment (bohr magnetron)
O7	2	2.449
N9	1	1.414
Total magnetic moment		3.863

Table 4(b). Magnetic susceptibility of 3-Dimethylaminoanisole at various temperatures.

S.NO	Temp. (kelvin)	Susceptibility(χ_m) mole per m^3	1/Temp. ($Kelvin^{-1}$)
1	50	4.5E-07	0.02000
2	100	2.3E-07	0.01000
3	150	1.5E-07	0.00667
4	200	1.1E-07	0.00500
5	250	9.0E-08	0.00400
6	298.5	7.5E-08	0.00335
7	350	6.4E-08	0.00286
8	400	5.6E-08	0.00250
9	450	5.0E-08	0.00222
10	500	4.5E-08	0.00200
11	550	4.1E-08	0.00182
12	600	3.8E-08	0.00167

Magnetic susceptibility (χ) is the primary measurement. This measures the strength of interaction of placing the substance in a magnetic field. In paramagnetic Materials χ is positive that is, for which M is parallel to B. The susceptibility is very small: 10^{-4} to 10^{-5}. The fact that these compounds have incomplete atomic shells is what is responsible for their paramagnetic behaviour. They all have a critical below which the variation of susceptibility with temperature is very different from its variation above this temperature. A paramagnetic compound will have some electrons with unpaired spins. A plot of χvs 1/ temperature is known as a Curie plot. Ideally, it should be linear if the Curie- Weiss law is obeyed. For the title compound the plot of χvs 1/T is linear hence Curie-Weiss law is obeyed. From such a plot, we can then extract the Curie constant from the slope and the Weiss constant from the x-Intercept [27]. For 3DMA, Table 4(b)shows the variation of susceptibility with temperature and Fig. 4 shows the Curie pilot. The plot shows that 3DMA is paramagnetic in nature. The following linear equation (regression equation) is considered to be the best fit to predict the value of Curie constant

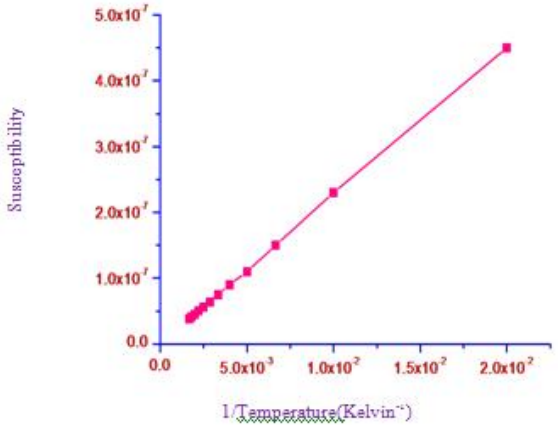

Fig. 4 Magnetic susceptibility plot of 3-Dimethylaminoanisole.

$Y = -2.56439 X10^{-10} + 2.25814 X10^{-5} X$ R= 0.99991

Curie constant = 0.0000225, Weiss constant = 5.12379×10^{-07} (BM).The Weiss constant is almost zero. Hence the plot passes through the origin which proves the paramagnetic nature of 3DMA. For the compound that obey the Curie law, the effective magnetic moment is independent of temperature.

5. Designed dyes

This study was carried out to design new sensitizers for DSSC applications. The designed dyes consist of following parts: donor (D), pi-spacer (pi), and acceptor (A) as shown in Fig.5(a). New dyes were designed by the structural modification of 3- Dimethylaminoanisole. Structure of 3DMA dyes are given in Fig 5(b). In these structures, benzene and triphenylamine (TPA) were used as electron-donating moiety and carboxyl, cyano and nitro groups (-COOH, -CN and $-NO_2$) were introduced as the electron acceptor and the anchor groups because of their high ability of electron- withdrawing and bonding to semiconductor. While 3-Dimethylaminoanisole were introduced as pi- conjugation to bridge the donor-acceptor systems.

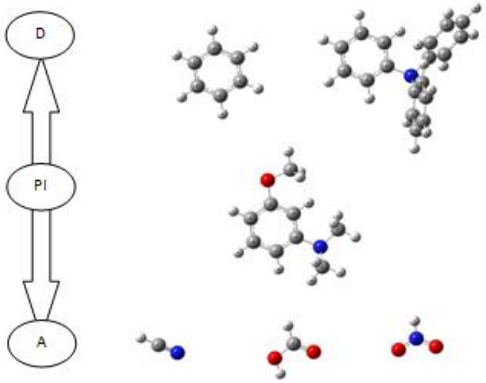

Fig. 5(a) Different parts of Donor – Pi spacer – Acceptor.

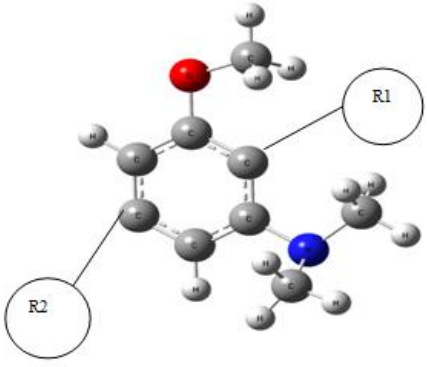

Fig. 5(b) Chemical structures of 3-Dimethylaminoanisole for newly designed dyes.

R1 = Benzene, Tiphenylamine R2 = CN, COOH, NO_2

5.1 HOMO, LUMO and Band gaps:

The HOMO, LUMO energy levels and band gaps Δ_{H-L} are computed, and the results are given in Table 5. From the table, with the increasing conjugated units, HOMO energy levels and LUMO energy levels decreased obviously, and the band gaps Δ_{H-L} present a decreased tendency. Moreover, it can be seen in Fig.6.Gauss-sum 2.2 program Boyle et al. [28] were used to calculated group contributions to the molecular orbital (HOMO and LUMO) and prepare the density of states (DOS) spectrum.Fig.6(a)shows the frontier molecular orbital energies and corresponding density of states spectrum of 3-Dimethylaminoanisole.Both the HOMO and LUMO energy levels of all dyes are slightly up-shifted is shown in Fig. 6(b) &6(c). The HOMO levels (-5.136 eV to -6.553 eV) of 3DMA dye 1-6 match well with the redox potential of the electrolyte system, which confirms the capability of dye regeneration from its oxidation state. The HOMO-LUMO energy gaps of the dye 6 is narrow on the order of 2.719 eV. The orbital density analysis of the HOMOs and LUMOs of the dyes reveals that homo orbitals are delocalized over the π-conjugated systems of benzene and TPA donors and extended along the π-linker to the central region of the molecule, while LUMO orbitals are also distributed across the π-linker and the anchoring group. This result shows that the substitution by TPA moiety decreases the gap energy more than the substitution with benzene moiety. This means that band gap Δ_{H-L} decreases by increasing the pi conjugation.

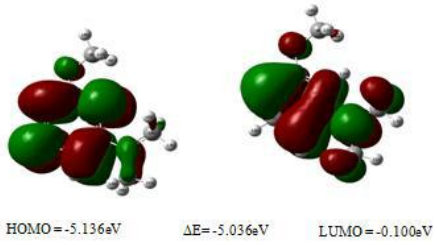

Fig. 6. HOMO-LUMO plot of 3-Dimethylaminoanisole

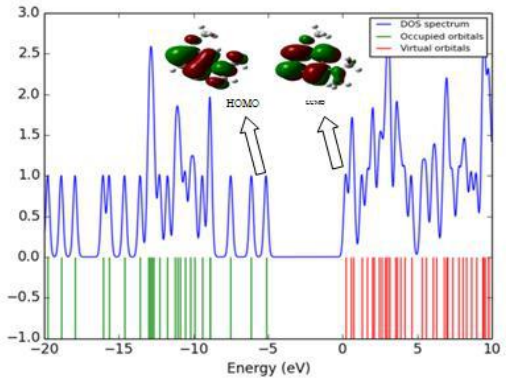

Fig.6(a) Density of states (DOS) diagrams for 3dma

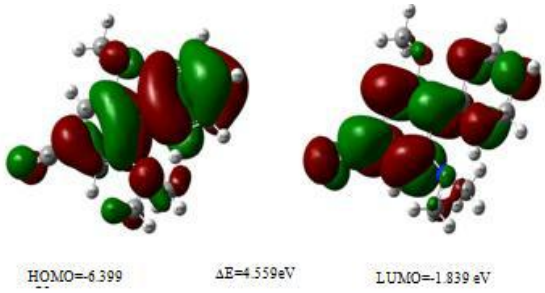

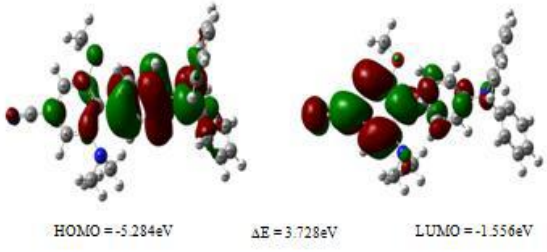

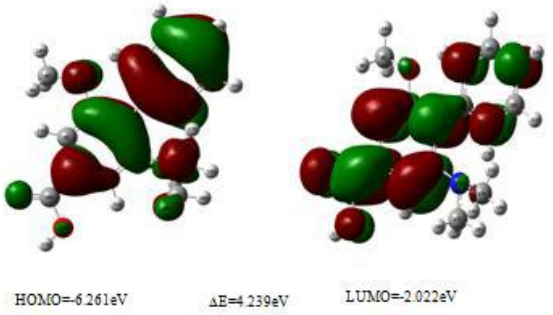

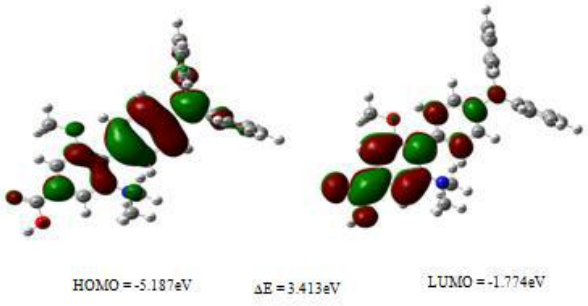

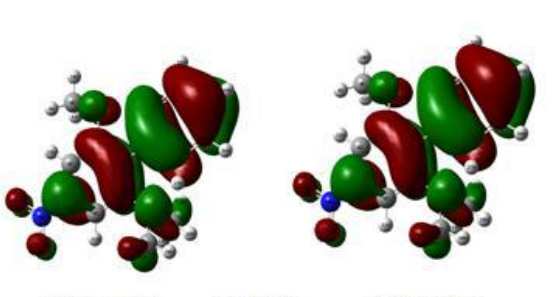

Fig. 6(b) HOMO, LUMO plot of 3dma with benzene as donor and acceptors

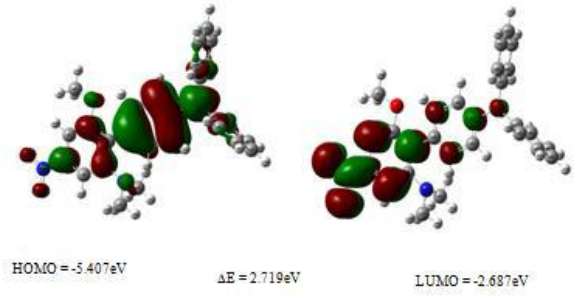

Fig. 6(c) HOMO, LUMO plot of 3-Dimethylaminoanisole with TPA as donor

5.2 Quantum chemical investigation

A chemical system is a collection of nuclei and electrons, it is used to understand the importance of electronegativity and chemical hardness. Hence it might be an atom, a molecule, an ion, or a cluster of many molecules that are in a state of chemical interaction. The DFT describes the physical and chemical behaviours of such systems [29, 30].

In this electronic chemical potential (μ) or absolute electronegativity (χ) and chemical hardness (η) are of explicit importance to understand regarding the electronic properties [31, 32]. Chemical potential measures the escaping tendency of an electron cloud, whereas Hardness, and has been outlined as the second partial derivative with reference to the quantity of electrons. It measures the resistance of an atom to a charge transfer and therefore the (global) softness S, is solely the inverse of global hardness, and describes the capability of an atom to receive electrons. As seen from the Table 5, the chemical hardness of 3DMA is high in gas phase, whereas introducing donors and acceptors substituents in 3DMA, it's minimized. Comparatively dye 3DMA 6 has lowest hardness value out of six derivatives of 3DMA. This decrease in chemical hardness is because of the presence of donor triphenylamine and acceptor NO_2.

Table 5. Quantum Chemical Parameters and Back donation of 3-Dimethylaminoanisole calculated at B3LYP/ 6-31+G(d, p) basis set.

Parameters	Values (eV)						
	3DMA	3DMA - DYE1	3DMA - DYE2	3DMA - DYE3	3DMA - DYE4	3DMA - DYE5	3DMA - DYE6
Ionization potential (IP)	-5.136	-6.399	-6.261	-6.553	-5.284	-5.187	-5.407
Electron affinity (EA)	-0.100	-1.839	-2.022	-2.941	-1.556	-1.774	-2.687
Energy gap	5.036	4.560	4.239	3.612	3.728	3.413	2.720
Hardness(η)	2.518	2.280	2.120	1.806	1.864	1.707	1.360
Softness(S)	0.199	0.219	0.236	0.277	0.268	0.293	0.368
Chemical potential(μ)	-2.618	-4.119	-4.142	-4.747	-3.420	-3.481	-4.047
Electrophilicity index (ω)	1.361	3.721	4.046	6.239	3.137	3.549	6.021
Charge Transfer (ΔN_{max})	1.040	1.807	1.954	2.628	1.835	2.040	2.976
Nucleofugality (ΔEn)	1.460	5.560	6.068	9.180	4.693	5.323	8.708
Electrofugality (ΔEe)	6.497	10.120	10.307	12.792	8.421	8.736	11.428

Back donation($\Delta E_)$	-0.630	-0.570	-0.530	-0.452	-0.466	-0.427	-0.340

Electronegativity (χ) describes the potential of an atom in a molecule to draw in electrons. Mulliken outlined electronegativity as the average of ionization potential (IP) and electron affinity (EA). For atomic species the chemical potential is that the negative of Mulliken electronegativity (χ) which may conjointly name as absolute electronegativity. That is, the resistance of the chemical potential to a modification within the range of electrons.

The definition of μ and η be drawn as, - $\mu = (IP+EA)/2 = \chi$; $\eta = (IP-EA)/2$,

According to Koopmans's theorem [33] the ionization potential (IP) and lepton affinity (EA) of the compound are calculated using the subsequent equations.-E_{HOMO} = IP, -E_{LUMO} = EA;

The higher HOMO energy relates to a lot of reactive molecule within the reactions with electrophile, whereas lower LUMO energy is crucial for molecular reactions with nucleophiles.Hard molecules have an enormous HOMO-LUMO gap, and soft molecules have a tiny HOMO-LUMO gap. In equilibrium chemical hardness could be a function of position. Consistent with Sanderson's [34] electronegativity, absolute electronegativity within a chemical system is equal all over, whereas equalization principle, once 2 systems, A and B, are brought along, electrons can be due from lower χ to higher χ till the chemical potential reaches equilibrium. As a primary approximation, the fractional range of electrons transferred, Charge transfer ΔNmax, is given by

$$\Delta Nmax \approx \frac{\Delta\chi}{2\Sigma\eta} \quad \text{(or)} \quad \Delta Nmax \approx -\frac{\Delta\mu}{2\Sigma\eta}$$

Thus, the electron transfer is driven by Δχ, however resisted by the total of hardness. Charge transfer is not the entire modification of electrons however continues to be helpful in determining the orbital interaction between 2 chemical systems, and in serving as approximation for the bond length [30]. For the hard – hard interactions, hardness (η) are often very large; so ΔN becomes too tiny, and therefore the interaction are dominated by the static interaction, rather than electron (charge) transfer. For the soft – soft interactions, η are often rather tiny and so ΔN becomes overlarge. Such interactions can have sturdy implications within the interaction, rather than electron (charge) transfer (ΔNmax). Table 5 shows the values of ΔN calculated for variety of designed dyes. Consistent with Klopman'spolyelectronic perturbation theory regarding electron transfer between donors and acceptors, two major terms are concerned within the acid-base interaction: the coulombic and the frontier orbital [35].

The inhibition potency of the molecules 3DMA and their dyes obtained quantum chemically increase with the rise in E_{HOMO}, and reduce in energy gap (ΔE). 3DMA dye6 has the very best inhibition potency as a result of it had the highest charge transfer values and lowest energy gap and hardness it absolutely was most capable of providing electrons and it might have a far better performance corrosion matter.

5.3 Nonlinear Optical Effects

The first hyperpolarizability provides the second order of response to the applied electric field, being of great importance in NLO. In this work, diploe moment, polarizability and first hyperpolarizability of 3DMA are explored using a density functional theory. The connection between the electric dipole moments of an organic molecule having donor-acceptor substituent and first order hyperpolarizability is typically recognized in the literature [36]. Therefore, the compounds with Donor-Acceptor configuration are the established molecules for quadratic hyperpolarizability, which were also found to exhibit two or three photon absorption cross-sections. Since intramolecular charge-transfer interactions during photo excitation, such molecules are deliberated as promising candidates for

designing organic solar cell [37].The present results indicate that these properties are strongly sensitive to the electronic structure of the title compound. Dipole moment and polariazability are electron properties with great importance in structural chemistry. It allows to compare the evolution of β_{total} and energy gap from 3DMA to their dyes and reveals an interesting relation between these properties. Hyperpolarizability is related to an intramolecular charge transfer process, and low energies favour this property. It is premise that NLO materials have moderate HOMO-LUMO gap.

Table 6. Nonlinear optical properties of 3-Dimethylaminoanisole performed at 6-31+G(d, p).

Parameters	3DMA		Dye1	Dye 2	Dye 3	Dye 4	Dye 5	Dye 6
	B3LYP							
	6-31+g(d,p)	cc-pVTZ						
μ_{tot}	3.1823	3.2009	2.782	1.7934	3.4494	5.0659	2.4947	6.1672
Δα(esu)	-64.636	-64.58	-118.3259	-117.0445	-122.8996	-193.811	-186.569	-199.244
βtot(esu)	2.526E-30	2.565E-30	1.731E-29	3.87E-30	9.697E-30	4.708E-29	5.687E-30	3.674E-29

The vertical transition dipole moment of the dye was assessed to provide a better understanding of the performance of the Intramolecular Charge Transfer (ICT) upon photo excitation. From Table 6. the calculated diploe moment values of dyes are on the order of 6.1672, 5.0659, 3.4494, 3.1823, 2.782, 2.4947, 1.7934 Debye for dye6, dye4, dye 3, 3DMA, dye1, dye 5, dye 2 respectively. The highest value of dipole moment is dye 6 suggesting the highest capability of electron injection driving force from the absorbed dye 6 into the TiO_2 substrate. Notably, with respect to 3DMA addition with TPA and NO_2. Overall, the calculated results clearly explain the dye6 is the most efficient dye among its sister dyes. Adding TPA unit to the dye could improve the electron injection driving force in the device than the benzene moiety.

6. ELECTRONIC AND PHOTOVOLTAIC PROPERTIES

6.1. Open Circuit Voltage (v_{OC})

The charge collection efficiency (η) is determined by the short-circuit current density (J_{sc}), the open-circuit photovoltage (v_{oc}), the fill factor (FF) and incident solar power. The charge collection efficiency (η) can be calculated [38] using the equation.

$$\eta = \frac{J_{SC} FF \text{voc}}{P_{inc}}$$

The open circuit voltage(v_{OC}) of organic solar cells is linearly related with the HOMO of the donor and LUMO of the acceptor. The difference between the HOMO of the dye and the LUMO of the electron acceptor, phenyl-C_{61}-butyric acid methyl easter [PCBM] or to the conduction band of semiconductor TiO_2. The open circuit voltage was calculated by the following expressions [39,40],$v_{OC} = [|E_{HOMO}(D)| - |E_{LUMO}(A)|]$ -0.3 V

Where as in Dye sensitized Solar Cells (DSSC), v_{OC} might be calculated as the difference of energy between LUMO of the dye and conduction band of semiconductor TiO_2, voc $= E^{dye}_{LUMO} - E_{CB}$

Table 7 shows the calculated values of open circuit voltage and these values are positive and it explains that electron transfer will be easy from the title compound and its dyes 3DMA1 – 3DMA6 to acceptor. In addition, these values are enough to get the high capable electron injection. Further one parameter (α_I) determined by the difference between the LUMO energy levels of the 3DMA dyes and the

LUMO energy level of PCBM [41]. $\alpha_i = E_{LUMO}^{Acceptor} - E_{LUMO}^{Donor}$. The obtained values is shown in Table 7. It was in the range (0.859 - 3.600 eV). This indicates that all LUMO level from all 3DMA dyes is situated at LUMO level of PCBM.

6.2. Exciton Binding Energy (EBE):

The exciton binding energy reveals that the dyes with lower EBE values produce electric current from the absorbed photons more efficiently [42]. This is an important for charge collection efficiency and also electroluminence quantum efficiency of optical light emitting diodes [43, 44] can be determined by the following equation:$EBE = \Delta E_{L-H} - \lambda_{max}^{Abs}$, Here $\Delta E_{L\text{-}H}$ is the HOMO-LUMO energy gap. λ_{max}^{Abs} describes the maximum excitation energy. The calculated values of EBE is shown in Table 7. It outlined that 3DMA4 has the lowest exciton binding energy compared to other designed dyes.

Table 7. Energy values of the open circuit voltage - Voc (eV), light harvesting efficiency (LHE) of 3- Dimthylaminoanisole and its dyes.

Dyes	Wavelength (nm)	Excitation energy (eV)	Oscillator Strength	LHE	V_{oc}(eV)/PCBM	V_{oc}(eV)/Tio_2	α_I(eV)	EBE (eV)
3DMA	245	5.057	0.265	0.457	1.136	3.900	3.600	0.654
Dye 1	290	4.168	0.399	0.601	2.399	2.161	1.861	0.288
Dye 2	321	3.864	0.368	0.571	2.261	2.978	1.678	0.375
Dye 3	379	3.271	0.277	0.471	2.553	2.059	0.859	0.341
Dye 4	364	3.404	0.627	0.764	1.284	2.444	1.144	0.061
Dye 5	397	3.122	0.570	0.731	1.187	2.226	1.926	0.291
Dye 6	496	2.501	0.414	0.614	1.407	1.313	1.013	0.217

6.3. Electronic absorption spectra and sensitized mechanism

To gain insights into the excited states giving rise to the intense absorption spectra of sensitizers, TD-DFT calculations were performed at the B3LYP/ 6-31+G (d,p) level. Computed maximum absorption wavelength (λ_{max}), absorption energy, oscillator strength (f) and nature of the transitions are listed in Table 7. All dyes showed absorption moved from UV to visible region (290-500nm) is shown in Fig. 7. Absorbance in the visible region is required for high efficiency. Oscillator strength is in the range 0.2651 to 0.6274. Short –circuit photocurrent density (Jsc).

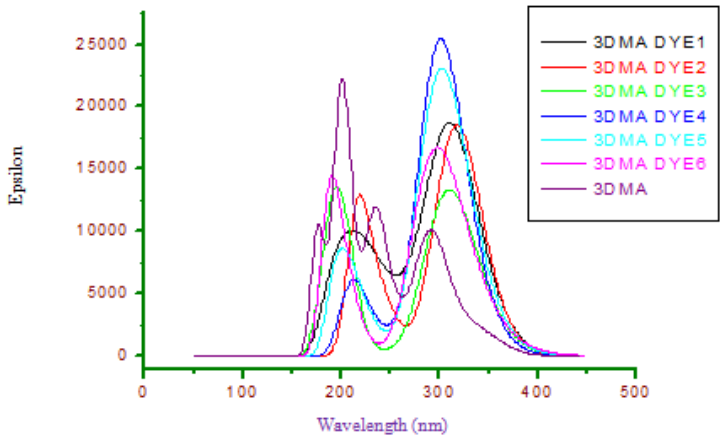

Fig. 7 UV absorption spectra of 3-Dimethylaminoanisole and its dyes.

The J_{sc} in dye sensitized solar cells is determined by $J_{sc} = \int LHE(\lambda)\, \Phi_{inject}\, \eta_{collect}\, d\lambda$

Where LHE is the light harvesting efficiency at a given wavelength, Φ_{inject} is the electron injection, and $\eta_{collect}$ is the charge collection efficiency. It is reasonable to assume that charge collection efficiency is a constant. Then, the enhancement of J_{sc} should focus on improving LHE and Φ_{inject} . In order to obtain a high J_{sc}, the efficient organic dyes used in DSSCs should have a large LHE.

6.4. Light Harvesting Efficiency (LHE)

Light harvesting efficiency (LHE), as an indicator of the incident photon to current conversion efficiency (IPCE), characterizes the capability of dyes in harvesting light. The LHE can be approximately expressed as [45]

$LHE = 1\text{-}10^{-A} = 1\text{-}10^{-f}$

Where A(f) is the absorption (oscillator strength) of the dye associated with the λ_{max}, that is, the lowest vertical excitation energy (E). Table 7 lists the lowest vertical excitation energies E, oscillator strengths (f), and relative LHE of all dyes. According to the structural and spectral properties, the relative LHE is evaluated by comparing dyes. Dye 4 owns the highest LHE of 0.7642, followed by dyes in the order 5, 6, 1, 2, 3. This trend is in good agreement with the sequence of electron donating ability of heteroatoms involved. For 3, 4 and 5 in TPA donor, 4 shows the highest LHE of 0.7642, followed by 5 of 0.7310 and 4 of 0.6143.

6.5. Electron injection efficiency:

Another way to improve short-circuit photo current density J_{sc} is to improve Φ_{inject} which is related to the driving force (ΔG^{inject}) of the electron injection from the photo induced excited states of organic dyes to the Tio_2 surface. In general, a larger ΔG^{inject} leads to a larger Φ_{inject} .

The calculation of electron injection quantities is important for the interpretation of photovoltaic data. The calculated ΔG^{inject}, as well as E_{ox}^{dye} and $E_{ox}^{dye\,*}$ for dyes [46-48] and the results are listed in Table 8. It was found that all the calculated ΔG^{inject}were negative, which means that the dye excited state lies above the TiO_2 conduction band edge, favouring the injection of the electron from the excited state dye to the TiO_2 conduction band edge. From Table 9 it is clear that ΔG^{inject}becomes more negative by adding electron deficient pi-spacers. Improvement in LHE and driving force (ΔG^{inject}) of the electron injection would show higher J_{sc}. Performance of DSSCs sensitized by dye4 might be superior to the other dyes.

Table 8. Electron injection efficiency of 3-Dimethylaminoanisole and its dyes 1 to 6.

Dyes	Eox^{dye}(eV)	Eox^{dye*}(eV)	λ_{max}^{ICT}(eV)	λ_{max}(nm)	ΔG^{inject}
3DMA	5.136	0.754	4.382	245	-3.256
Dye 1	6.399	2.128	4.271	290	-1.882
Dye 2	6.261	2.397	3.864	321	-1.613
Dye 3	6.553	3.282	3.271	379	-0.728
Dye 4	5.284	1.618	3.666	338	-2.392
Dye 5	5.187	2.065	3.122	397	-1.945
Dye 6	5.407	2.905	2.502	496	-1.105

7. CONCLUSION

The present study systematically analysed the vibrational spectra, both infrared and Raman of 3DMA. The complete vibrational assignments of wavenumbers are made on the basis of potential energy distribution (PED). The MESP map shows that the negative potential sites are on electronegative atoms and the positive potential sites are around the hydrogen atoms. These sites provide information

concerning the region from where the compound can undergo intra- and intermolecular interactions. Similarly the Fukui charges confirm the intermolecular hydrogen bonds. Besides, a theoretical investigation on organic sensitizers incorporating donors and acceptors units based on 3DMA and 3DMA dyes1-6 have been studied by TD-DFT/B3LYP 6-31+G(d,p) method. The predicted nonlinear optical properties of the complex are much greater than that of urea. The compound is a good candidate as second-order nonlinear optical materials.

DFT based quantum chemical parameters are considered: absolute electronegativity, chemical potential, and chemical hardness. From these parameters, a fundamental parameter ΔN has estimated. The title compound and its dyes showed their ability to inhibit the corrosion process could be established. The absorption spectra were evaluated. The systems substituted by TPA groups exhibit better results than benzene. The energy gaps were calculated. The theoretical values of open circuit voltage were calculated. The results obtained show that the absorption maxima of the studied systems vary between 245 to 496 nm, which is very suitable for an efficient harvest of light. The obtained results proved that the electronic properties can be tuned by the substituents with TPA - donor as good sensitizer for dye sensitized solar cell applications.

REFERENCES

[1] Brain O'Regan, M. Grätzel, Nature 1991, 353, 737-740.
[2]W.Xu,B.Peng, J.Chen,M.Liang, F.Cai, J. Phys. Chem. C, 2008, 112, 874-880.
[3] S.Hwang, J, H. Lee,C. Park,H. Lee, C. Kim, C. Park, M.H. Lee, W. Lee, J. Park, K. Kim, N.G. Park,C. Kim, Chem. Commun.. 2007, 4887-4889.
[4] E. Kraka,D.Cremer, J Am. Chem. Soc., 2000; 122: 8245-8264.
[5] P. HohenbergandW. Kohn, Phys Rev, 1964; B136; 864-871.
[6] R.G. Parr, and W. Yang, Density-Functional Theory of Atoms and Molecules. (Oxford university Press' New York, 1989).
[7] M.H. Cohen, In Topics in Current Chemistry; R.F. Nalewajski, Ed.; (Springer-Verlag: Heidel berg, Germany, 1996; 183: p 143.
[8] R.T. Sanderson R T, Am Chem Soc., 1952; 74, 272-274.
[9] M.K. Awad, J.Electroanal Chem., 2004; 567: 219-225.
[10] Robert G. Parr, and WeitaoYang , J. Am Chem Soc., 1984, 106(14),pp4049-4050.
[11] Ralph G. Pearson, J. Am. Chem. Soc. 1963; 85(22), 3533-3543.
[12] S. Venkatesan, Q. Chen, E.C .Ngo, N. Adhikari, K. Nelson, et al. (2014) Polymer solar cells processed using anisole as a relatively non-toxic solvent. Energy Technology 2: 269-274.
[13] M. Frisch, G.W. Trucks, H.B. Schlegal, G.E. Scuseria, M.A. Robb, J.R. Cheesman,V.G. Zakrzewski, J.A. Montgomerg, Jr., R.E. Strtmann, J.C. Burant, S. Dapprich, J.M.Milliam, A.D. Daniels, K.N. Kudin, M.C. Strain, O. Farkas, J. Tomasi, V. Barone,M. Cossi, R. Camme, B. Mennucci, C. Pomelli, C. Adamo, S. Clifford, J. Ochterski,G.A. Petersson, P.Y. Ayala, Q. Cui, K. Morokuma, N. Rega, P. Salvador, J.J.Dannenberg, D.K. Malich, A.D. Rabuck, K. Raghavachari, J.B. Foresman, J.Cioslowski, J.V. Ortiz, A.G. Baboul, B.B. Stetanov, G. Liu, A. Liashenko, P. Piskorz,I. Komaromi, R. Gomperts, R.L. Martin, D.J. Fox, T. Keith, M.A. Al-Laham, C.Y.Peng, A. Nsnsyskkara, M. Challacombe, P.M.W. Gill, B. Johnson, W. Chen, M.W.Wong, J.L. Andres, C. Gonzalez, M. Head-Gordon, E.S. Replogle, J.A. Pople,GAUSSIAN 09, Revision A.02, Gaussian, Inc, Pittsburgh, PA, 2009.
[14] J.B.Foresman, in: E. Frisch (Ed), Exploring chemistry with Electronic Structure Methods: A Guide to Using Gaussian, Pittsburg, PA,1996.
[15] R. Dennington, T. Keith, J. Millam, Gaussview, Version 5, semichem Inc., ShawneeMission KS, 2009.
[16]T. Sundius, J. Mol. Struct. 218 (1990) 321, 1-466.
[17] T. Sundius, Vib. Spectrosc. 29 (2002) 89-95.
[18] S. Ramalingam, S. Periandy, Spectrochem. Acta Part A 78 [2011] 835-843.
[19] M. Karnan, V. Balachandran, M. Murugan, M.k. Murali, A. Nataraj, SpectrochemActa Part A 116(2013) 84-95.
[20] C. Lee, W. Yang, R.G. Parr, Phys. Rev. B 37 (1988) 785.

[21] A.D. Becke, J. Chem. Phys. 98 (1993) 5648-5652.
[22] M. Silverstein, G. Clayton Basseler, C. Morill, Spectrometric Identification of Organic Compounds, Wiley, Newyork, 1981.
[23] S. Gunasekaran, S. kumerasan, R. Arunbalaji, S. Srinivasan, J. Chem. Sci. 120(3) 2008 315-324.
[24] W. Yang and W. J. Mortier, J. Am. Chem. Soc, 108 (1986) 5708-5711.
[25] R. S. Mulliken, J. Chem. Phys., 23 (1955) 1833.
[26] Wahid U. Malik, G.D. Tuli, R.D. Madan, Selected topics in Inorganic Chemistry, S. Chand & Company Ltd, New Delhi. 1996.
[27]M.C. Gupta, Atomic and Molecular Spectroscopy, New Age International Private Limited, Publishers, New Delhi, 2001.
[28] O'Boyle N.M., A.L. Tenderholt, K.M. Langner, cclib: A library for package-independent computational chemistry algorithms, J. Comput. Chem., 29 (2008) 839-845.
[29] Li, S. H.; Zhang, R. J.; Jin; Wang, Y. C.; Tung, S. C. Tribology Transactions 2003, 46, 200-205.
[30] R.G. Parr, R.G. Pearson, J. Amer. Chem. Soc. 1983, 105, 7512-7516.
[31] Pearson, R.G. Proc. Natl. Acad. Sci. 1986, 83, 8440-8411.
[32] L.H. Lee, Relevance of the density-functional theory to acid-base interactions and adhesion in solids, in Acid-Base Interactions (Eds. K. L. Mittal and H. R. Anderson, Jr.), VSP, Netherlands, 1991, 25-46.
[33] T. Koopmans, Physica 1 (1934) 104-113.
[34] R.T. Sanderson, J. Am. Chem. Soc., 1952; 74, 272-274.
[35] G. Klopman, J. Amer. Chem. Soc. 1968, 90, 223-234.
[36] S. Arulmozhi, M. Victor Antony Raj, J. Madhavan, Der ChemicaSinica 2, 158 – 163 (2011).
[37] J. Fortage, A. Scarpaci, L. Viau, y. Pellegrin, E. Blart, M. Falkenstrcm, L. Hammarstrcm, I. Asselberhs, R. Kellens, W. Libaers, K. Clays, M. P. Eng, F. odobel, Charge-transfer state and large first hyperpolarizability constant in a highly electronically coupled zinc and gold prophyrin dyad, Chem. Eur. J. 15 (2009) 9058-9067.
[38] Z. Guo, W. Liang, Y. Zhao, G. Chen, Real-time propagation of the reduced one-electron density matrix in atom-cantered orbitals; application to electron injection dynamics in dye sensitized TiO2 clusters, J. Phys. Chem. C 112 (42), 2008, 16655-16662.
[39] M. Bourass, et al., DFT/TD-DFT characterization of conjugational electronic structures and spectral properties of materials based on thieno[3,2-b][1]benzothiophene for organic photovoltaic and solar cell applications, J. Saudi Chem. Soc. (2017).
[40] M. Bourass, et al., DFT and TD-DFT calculation of new thienopyrazine-based small molecules for organic solar cells, Chem. Central J. 10 (2016) 67.
[41] M.C. Scharber, D. Mùhlbacher, M. Koppe et al., "Design rules for donors in bulk-heterojunction solar cells-towards 10% energy-conversion efficiency," Advanced Materials, Vol. 18, no. 6, pp. 789-794, 2006.
[42] Y. Li, T. Pullerits, M. Zhaao and M. Sun, J. Phyd. Chem. A1 (2013) 4358-4369.
[43] A. Franceschetti, A. Zunger, Phys. Rev. Lett. 78 (1997) 915-918.
[44] Y. Cao, I.D. Parker, G. Yu, C. Zhang, A.J. Heeger, Nature 397 (1999) 414-417.
[45] H.S. Nalwa, handbook of advanced electronic and photonic materials and devices; Academic San Diego, 2001.
[46] R. Katoh,; Furube, A.; Yoshihara, T.; Hara, K,; fujihashi, G.; Takano, S; Murata, S.; Arakwa, H.; Tachiya, M. J. Phys. Chem. B 2004 108,4818-4822.
[47] H.S. Nalwa, handbook of advanced electronic and photonic materials and devices; Academic San Diego, 2001.
[48] J. Preat,; C. Michaux,; D. Jacquemin, E. Perpete, A. J. Phys. Chem. C 2009, 113, 16821-16828.

M. Anuradha
PG& Research Department of Physics, Srimad Andavan Arts & Science College (Autonomous), Trichy, Tamil Nadu, India.